Analysis of Different Reference Plane Setups for the Calibration of a Mobile Laser Scanning System*

Erik HEINZ, Christian ELING, Markus WIELAND, Lasse KLINGBEIL
and Heiner KUHLMANN

1 Introduction

The discipline of engineering geodesy is currently subject to a paradigmatic change because the measuring of carefully selected single points is progressively replaced by an area-based acquisition of structures in form of a 3D point cloud. This development is closely linked to the improvements in laser scanning technology, which has become a standard measuring technique in engineering geodesy (KUHLMANN et al. 2014). In the recent past, also the acquisition of spatial 3D data by using mobile laser scanning systems has gained more and more acceptance. In this case, the environment is measured kinematically by using 2D laser scanners on moving platforms. The position and attitude of the platform is determined by additional sensors (e. g. a GNSS/IMU unit), but the measured point clouds can also be used to obtain information on the platform motion. Typical applications of such mobile systems are e. g. road surface inspection or the generation of data for 3D city or building models and infrastructural databases of roads and rail tracks. Good reviews of mobile surveying technologies and their applications can be found in PUENTE et al. (2013) or OLSEN et al. (2013). The development of mobile laser scanning systems imposes particular requirements, which include the fusion of the georeferencing sensors for the estimation of the platform trajectory by using special filter algorithms, a comprehensive understanding of the scanning process as well as the consistent integration of the stochastic models of all sensors. In addition to it, a precise time synchronization and a proper system calibration are crucial. While all aspects are vital to the success, this paper will solely focus on the system calibration.

1.1 Current calibration practice

The calibration parameters of a mobile laser scanning system can be classified into intrinsic and extrinsic parameters. Intrinsic parameters compensate for systematic deviations of the individual sensors and are usually determined at production in the laboratory. Regarding GNSS antennas, offsets and variations of the electrical phase center have to be calibrated, which can either be done by robot calibration methods (e. g. WÜBBENA et al. 2000) or in a anechoic antenna calibration chamber (e. g. ZEIMETZ & KUHLMANN 2008). The receiving characteristics of GNSS antennas are significantly influenced by its near-field. Thus strictly speaking, the GNSS antennas would have to be calibrated with the entire system. Regarding IMUs, which contain gyroscopes, accelerometers or magnetometers, the calibration of axial misalignments, biases and scale factors is crucial. This is usually done in the laboratory at a range of temperatures (TITTERTON & WESTON 2004, GROVES 2013). But a user-conducted calibration is also possible by performing special maneuvers (e. g. KLINGBEIL et al. 2014) or by estimating the scale factors and biases in a GNSS-aided trajectory filter algorithm during

* **Originally published in:** Heinz, E.; Eling, C.; Wieland, M.; Klingbeil, L.; Kuhlmann, H. (2017): *Analysis of Different Reference Plane Setups for the Calibration of a Mobile Laser Scanning System*, In: Lienhart, W. (Hrsg.): Ingenieurvermessung 17, Beiträge zum 18. Internationalen Ingenieurvermessungskurs, Graz, Österreich, S. 131-145, Wichmann Verlag, Berlin, Offenbach.

operation (e. g. ELING et al. 2015, MARTIN et al. 2016). In this study, the intrinsic calibration parameters of the georeferencing sensors will not be further discussed.

Laser scanners exhibit systematic deviations in the beam deflection unit and in the distance measurement, which are normally calibrated at production. A user-conducted calibration is also possible. However, this is an up-to-date research topic (HOLST et al. 2016). Regarding mobile systems, laser scanners are calibrated separately in the laboratory (e. g. GRÄFE 2007, HAUSER et al. 2016) or in combination with the extrinsic calibration parameters since both parameter sets can be deduced from a 3D point cloud. The extrinsic calibration of a mobile laser scanning system includes the lever arm and boresight angles between the laser scanner coordinate frame and the platform-fixed coordinate frame to which the position and attitude of the platform are referred (e. g. the axes of the IMU). In this context, many solutions exist that need a mechanic realization of the platform-fixed coordinate frame (e. g. GRÄFE 2007) or a 3D measuring mode of the laser scanner (e. g. TALAYA et al. 2004). Moreover, it is not clear to what extent these methods are adaptable to other systems.

In order to overcome these limitations, methods based on the scanning of reference planes were developed that use constraints between the reference planes and the scanned points to estimate intrinsic and extrinsic calibration parameters of the laser scanners. This arose from airborne laser scanning, where the boresight angles and range offsets of laser scanners were derived from the scanning of planar surfaces on the ground under varying flight maneuvers. While in FILIN (2003) the plane parameters were known from a terrestrial GPS surveying, SKALOUD & LICHTI (2006) estimated the plane parameters of roofs as auxiliary parameters. In either instance, the lever arm was separately calibrated in the laboratory. GLENNIE (2012) and HAUSER et al. (2016) applied the plane-based method to terrestrial systems by scanning building façades or street surfaces multiple times. Also the lever arm was estimated, but due to correlations not all components could be reliably determined. Yet, GLENNIE (2012) estimated intrinsic calibration parameters of the laser scanner. In HARTMANN et al. (2015) a laser tracker based system was calibrated by using reference planes. The plane parameters were determined with the laser tracker and the calibration was performed kinematically and statically, but still certain parameters were hard to determine. JIAN & RAVANI (2016) used a plane with a checkered pattern for the determination of the boresight angles. In CHAN et al. (2013) planes were expanded by catenaries, but solely the boresight angles were estimated. In RIEGER et al. (2010) and KELLER & STERNBERG (2013) special driving maneuvers past building façades or cylinders were performed to calibrate the boresight angles.

1.2 Main aspects of this study

The survey of the literature indicates that plane-based methods play a substantial role in the extrinsic and intrinsic calibration of mobile laser scanning systems, but also that they are often not able to determine all relevant parameters. Yet, this is not a problem of the plane-based method per se but of the network configuration, i. e. the setup of the reference planes and how they are scanned with the mobile system. In the case of an adequate configuration, all extrinsic parameters can be determined. Based on the works in HEINZ et al. (2015) and HEINZ et al. (2016) this contribution aims at analyzing and optimizing the network configuration of a plane-based approach for the calibration of the six extrinsic parameters and the range offset of a 2D laser scanner in a mobile laser scanning system by using simulations. The configuration is analyzed with different quality criteria like parameter covariances or

partial redundancies due to the analogy to geodetic networks (e. g. GRAFAREND & SANSÒ 1985, HOLST et al. 2013). This strategy has also been applied in the context of the calibration of terrestrial laser scanners by HOLST & KUHLMANN (2014).

The rest of this paper is structured as follows: Section 2 introduces the developed mobile laser scanning system. The system calibration approach is illustrated in Section 3. Section 4 addresses the analysis of the network configuration in the calibration field and presents real calibration results of the developed mobile laser scanning system, which are then evaluated in Section 5. Section 6 concludes with a résumé and gives an outlook on future activities.

2 Mobile laser scanning system

The developed mobile laser scanning system is shown in Figure 1. A small trolley serves as carrier platform although the system is adaptable to other platforms. The major components of the system are a 2D laser scanner Z+F Profiler 9012A (ZOLLER+FRÖHLICH 2016) and a navigation-grade inertial navigation system (INS) iMAR iNAV-FJI-LSURV (IMAR 2016).

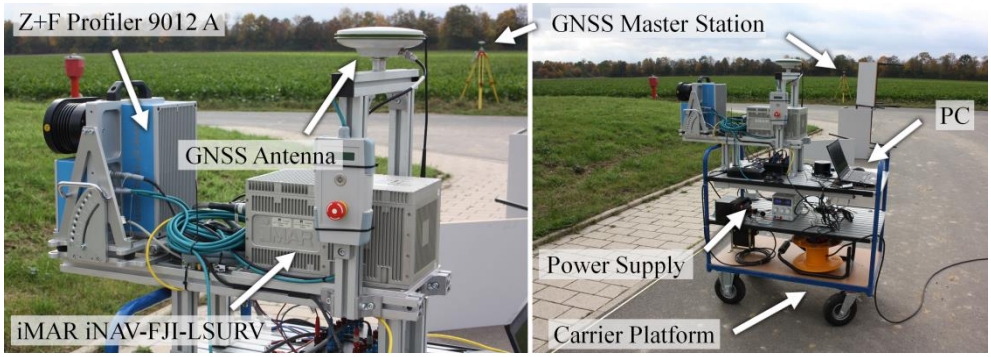

Fig. 1: Mobile laser scanning system consisting of a 2D laser scanner Z+F Profiler 9012A (ZOLLER+FRÖHLICH 2016) and an INS iMAR iNAV-FJI-LSURV (IMAR 2016).

The Z+F Profiler 9012A is a phase-based 2D laser scanner specially designed for kinematic applications. The instrument senses the object space in a 360° field of view in a range up to 119 m. The laser scanner is specified with an angular accuracy of 0.02° (root-mean-square) and range accuracy in the order of mm (standard deviation). The range accuracy depends on the measuring distance, the reflection properties of the surface and the scan rate, which can be set to a maximum of 1016 kHz and a rotational speed of the deflection mirror of 200 Hz. A special characteristic of the device is a special close-range-mode that optimizes the range noise in the distances between 1 m and 5 m. The iMAR iNAV-FJI-LSURV is a customized navigation-grade INS equipped with three fiber-optic gyroscopes and servo accelerometers with a maximum data rate of 1.5 kHz. The INS includes a triple-frequency + L-band GNSS receiver NovAtel OEM628 that is able to track all GNSS and allows for the calculation of a precise RTK-GNSS position if connected to a master station. The INS outputs raw data and a filtered platform trajectory. The accuracy of the attitude is specified with < 0.025° for the yaw angle and < 0.01° for roll and pitch angles if pure inertial data is used. In the GNSS-

aided case under good conditions and sufficient motion < 0.01° and < 0.002° are reached. The accuracy of the position is expected to be < 3 cm (practical value for RTK-GNSS). For the time synchronization the PPS (Pulse per Second) of the NovAtel GNSS receiver is used, which is a high-precision 1 Hz trigger pulse. To each pulse a message with a GPS time stamp belongs. The PPS is fed from the GNSS receiver into the INS processing unit and the observations of the GNSS receiver as well as those of the gyroscopes and accelerometers can be synchronized with the GPS time. In addition, the INS has a PPS output connector and the Z+F Profiler 9012A is equipped with a corresponding PPS input connector. Hence, the GPS time information can also be transferred to the 2D laser scanner.

3 Calibration approach

In this work, the system calibration comprises the determination of the range offset and the extrinsic calibration parameters of a 2D laser scanner in a mobile laser scanning system. In this context, different coordinate frames are important, which are summarized in Figure 2. Equation (1) shows the transformation of a scanned point from the local coordinate frame of the 2D laser scanner (s-frame) to the superior and georeferenced target coordinate frame (e-frame). In general, the item $\boldsymbol{R}$ denotes a rotation matrix.

$$\begin{bmatrix} x_e \\ y_e \\ z_e \end{bmatrix} = \begin{bmatrix} t_{xe} \\ t_{ye} \\ t_{ze} \end{bmatrix} + \boldsymbol{R}_n^e(L,B)\,\boldsymbol{R}_b^n(\phi,\theta,\psi) \left(\boldsymbol{R}_s^b(\alpha,\beta,\gamma) \begin{bmatrix} (d+d_0)\cdot\cos a\cdot\sin b \\ (d+d_0)\cdot\sin a\cdot\sin b \\ (d+d_0)\cdot\cos b \end{bmatrix} + \begin{bmatrix} \Delta x \\ \Delta y \\ \Delta z \end{bmatrix} \right) \quad (1)$$

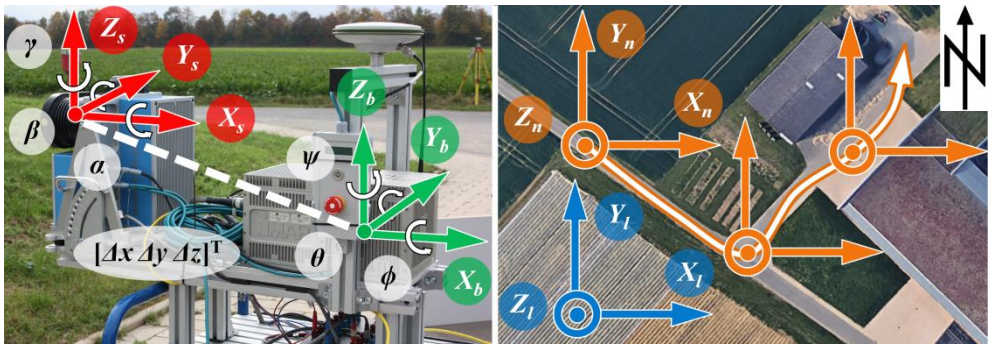

Fig. 2: Coordinate frames in the context of mobile scanning: **s**canner-frame, **b**ody-frame, **n**avigation-frame, local-**l**evel-frame and **e**arth-frame (e. g. WGS84, not depicted).

The points of the 2D laser scanner are initially given in its local coordinate frame (**s**canner-frame) and can be calculated from the polar elements, i. e. distance d, horizontal angle a and vertical angle b. The item d_0 is the range offset of the 2D laser scanner. The scanning plane of the 2D laser scanner is the Y_sZ_s-coordinate plane. Thus, in theory, all horizontal angles a have a constant value of 90°. However, the observed positions and attitudes of the INS are referred to a platform-fixed coordinate frame (**b**ody-frame), which often coincides with the axes of the IMU. The transformation between s-frame and b-frame is given by the lever

arm $[\Delta x, \Delta y, \Delta z]^T$ and the boresight angles α, β and γ (Figure 2). Beside the range offset d_0, these six extrinsic parameters have to be determined in the course of the system calibration. By using the attitude of the INS (i. e. roll ϕ, pitch θ and yaw ψ) the points can be rotated into the leveled and north-oriented **n**avigation-frame, whose origin coincides with the b-frame. Finally, the points are georeferenced in a superior **e**arth-frame (e. g. WGS84) by rotating them about the ellipsoidal latitude B and longitude L and then shifting them with $[t_{xe}\ t_{ye}\ t_{ze}]^T$, which is the observed position of the INS. However, the superior coordinate frame can also be a local-**l**evel-frame (Figure 2). In this case the rotation about B and L can be omitted.

In the following, the basic idea of the plane-based calibration approach is outlined, which is methodically similar to those surveyed in Section 1.1. More details can be found in HEINZ et al. (2015). The approach utilizes several differently oriented reference planes (Figure 6). The planes are georeferenced in a superior coordinate frame (e-frame or l-frame), e. g. with a 3D laser scanner in combination with control points. If the l-frame is located in the origin of the 3D laser scanner, the points on the plane surfaces must satisfy Equation (2), where s_l, z_l and h_l denote the polar elements of a scan point. Note that the normal vectors $[\tilde{n}_x, \tilde{n}_y, \tilde{n}_z]^T$ of the reference planes are scaled with the orthogonal distance between the plane and the origin of the coordinate frame, i. e. $\| [\tilde{n}_x, \tilde{n}_y, \tilde{n}_z] \| \neq 1$.

$$\begin{bmatrix} s_l \cdot \sin z_l \cdot \cos h_l \\ s_l \cdot \sin z_l \cdot \sin h_l \\ s_l \cdot \cos z_l \end{bmatrix}^T \begin{bmatrix} \tilde{n}_x \\ \tilde{n}_y \\ \tilde{n}_z \end{bmatrix} - 1 \overset{!}{=} 0 \tag{2}$$

The reference planes are then scanned with the mobile laser scanning system from various static stations in order to eliminate errors in the time synchronization and reduce noise (in principle kinematic scanning is also possible). The scanned points of the mobile system in the l-frame must satisfy the plane equations in Equation (3).

$$\left[\begin{bmatrix} t_{xl} \\ t_{yl} \\ t_{zl} \end{bmatrix} + \boldsymbol{R}_b^n(\phi,\theta,\psi) \left(\boldsymbol{R}_s^b(\alpha,\beta,\gamma) \begin{bmatrix} (d+d_0) \cdot \cos a \cdot \sin b \\ (d+d_0) \cdot \sin a \cdot \sin b \\ (d+d_0) \cdot \cos b \end{bmatrix} + \begin{bmatrix} \Delta x \\ \Delta y \\ \Delta z \end{bmatrix} \right) \right]^T \begin{bmatrix} \tilde{n}_x \\ \tilde{n}_y \\ \tilde{n}_z \end{bmatrix} - 1 \overset{!}{=} 0 \tag{3}$$

Equation (2) and (3) can be used as observation equations in a total least squares algorithm to estimate the calibration parameters $\boldsymbol{p}$ including their covariance matrix $\boldsymbol{\Sigma}_{pp}$. The item $\boldsymbol{p}_0$ denotes an approximate parameter vector because the adjustment problem is not linear. The normals of the reference planes are modeled as auxiliary parameters. The matrices $\boldsymbol{A}$ and $\boldsymbol{B}$ contain the partial derivatives of the constraints with respect to the parameters and observations, respectively. The matrix $\boldsymbol{\Sigma}_{ll}$ denotes the covariance matrix of the observations and the item $\boldsymbol{w}$ is the vector of discrepancies. According to MIKHAIL & ACKERMANN (1976), the Gauß-Helmert model is transformed to a Gauß-Markov model, i. e. $\boldsymbol{\Sigma}_{ll} = \boldsymbol{B}\,\boldsymbol{\Sigma}_{ll}\,\boldsymbol{B}^T$.

$$\boldsymbol{p} = \boldsymbol{p}_0 + \left(\boldsymbol{A}^T \boldsymbol{\Sigma}_{\tilde{l}\tilde{l}}^{-1} \boldsymbol{A} \right)^{-1} \boldsymbol{A}^T \boldsymbol{\Sigma}_{\tilde{l}\tilde{l}}^{-1} \boldsymbol{w} \tag{4}$$

$$\boldsymbol{\Sigma}_{pp} = \left(\boldsymbol{A}^T \boldsymbol{\Sigma}_{\tilde{l}\tilde{l}}^{-1} \boldsymbol{A} \right)^{-1} \tag{5}$$

4 Calibration Results

4.1 Calibration results on simulated data

4.1.1 Simulation of different reference plane setups

The network configuration in the calibration field (i. e. the setup of the reference planes and how they are scanned with the mobile system) is crucial for the quality of the calibration. In order to analyze and optimize the network configuration, a simulator was developed that allows for a simulation of arbitrary network configurations. By using the robotic simulation environment V-REP (COPPELIA ROBOTICS 2016) it is possible to design a calibration field and generate artificial observations of a mobile laser scanning system (Figure 3). This data can then be exported to an in-house developed MATLAB® software package, where the calibration algorithm as described in Section 3 is implemented and can be investigated.

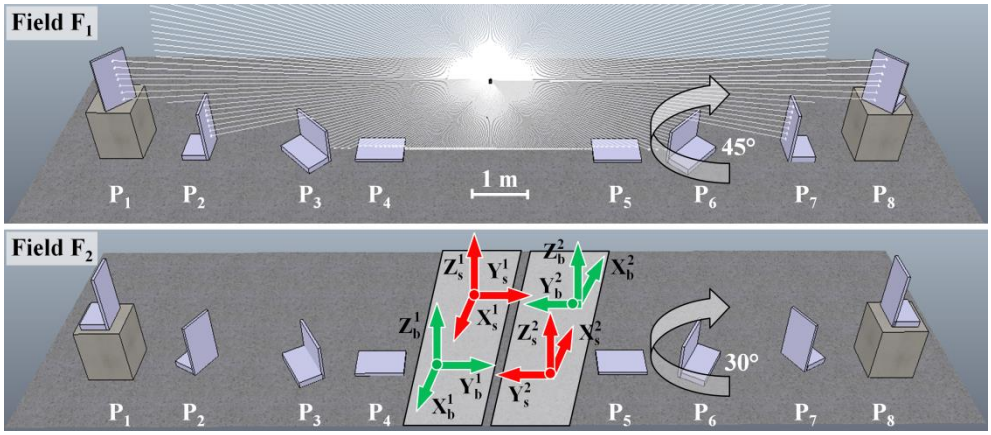

Fig. 3: Simulation of two calibration fields F_1 and F_2. For reasons of clarity, beside the reference planes P_k, only the scanning plane of the 2D laser scanner in F_1 and the s-frames and b-frames of two diametrical stations S_1 and S_2 in F_2 are depicted.

In Figure 3 two simulated calibration fields F_1 and F_2 can be seen, both with eight reference planes P_k (0.6 m × 0.9 m). In field F_1 the planes $P_{1, 3, 6, 8}$ and in field F_2 the planes $P_{2, 3, 6, 7}$ were rotated by 45° and 30° with respect to their vertical axis, respectively. Moreover, six static stations S_j of the mobile laser scanning system were simulated in each field, i. e. the system calibration is always based on the joint analysis of six static scans. In addition, two different configurations were simulated in each field. In the first configuration all six stations had an identical attitude (F_{1a} and F_{2a}) and in the second configuration three stations had a diametrical attitude (F_{1b} and F_{2b}), i. e. the system was turned by 180° with respect to the vertical axis (Figure 3, bottom panel). Thus, all in all, four different configurations were analyzed. Basically, the calibration procedure can also be performed by scanning the planes kinematically. The static procedure aims at eliminating potential errors in the time synchronization and at reducing noise because in reality (Section 4.2) the individual stations can be measured for a certain time and the position and attitude observations can be averaged. In

the simulation, the noise of the observations was generated according to manufacturer specifications, which are summarized in Table 1. Following this, the calibration procedure was executed for the four simulated configurations (F_{1a}, F_{1b}, F_{2a} and F_{2b}). By running a Monte Carlo experiment it was verified that the estimation of the calibration parameters within the simulation is unbiased.

Table 1: Standard deviations (STD, 1σ) of the observations as used in the simulation.

Observation	t_{xl} t_{yl} t_{zl}	ϕ θ ψ	d	b	s_l	z_l	h_l
STD (1σ)	0.01 m	0.01°	0.0003 m	0.02°	0.001 m	0.0025°	0.0025°

4.1.2 Analysis with accuracy criteria

Different criteria were utilized to assess the quality of the calibration results. Table 2 shows the accuracies of the estimated calibration parameters for the four simulated configurations. The lever arm $[\Delta x, \Delta y, \Delta z]^T$ as well as the boresight angles α and γ have the same accuracy for all four configurations. This accuracy depends on the accuracy of the position and attitude observations of the mobile laser scanning system and is reduced by the square root of the number of stations S_j, which is six in this case. Thus, the accuracy of the parameters is improved by a factor of $\sqrt{6} \approx 2.45$ in relation to the observations (Equation (6)).

$$\sigma_{\alpha,\beta,\gamma} = \frac{\sigma_{\phi,\theta,\psi}}{\sqrt{\sum S_j}}, \quad \sigma_{\Delta x,\Delta y,\Delta z} = \frac{\sigma_{t_{xl},t_{yl},t_{zl}}}{\sqrt{\sum S_j}} \tag{6}$$

Table 2: Standard deviations (STD, 1σ) of the estimated calibration parameters for the four network configurations (F_{1a}, F_{1b}, F_{2a} and F_{2b}) in the simulation.

Parameter	$\sigma_{\Delta x}$	$\sigma_{\Delta y}$	$\sigma_{\Delta z}$	σ_{α}	σ_{β}	σ_{γ}	σ_{d0}
F_{1a} (identical)	0.0041 m	0.0041 m	0.0041 m	0.0041°	**0.0046°**	0.0041°	0.02 mm
F_{2a} (identical)	0.0041 m	0.0041 m	0.0041 m	0.0041°	**0.0070°**	0.0041°	0.02 mm
F_{1b} (diametrical)	0.0041 m	0.0041 m	0.0041 m	0.0041°	**0.0042°**	0.0041°	0.01 mm
F_{2b} (diametrical)	0.0041 m	0.0041 m	0.0041 m	0.0041°	**0.0058°**	0.0041°	0.01 mm

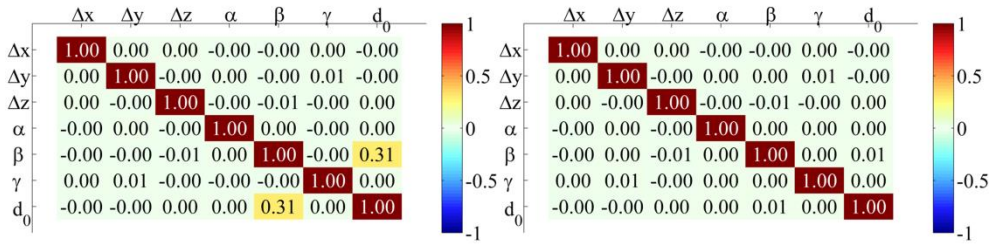

Fig. 4: Correlations of the calibration parameters for the two configurations F_{1a} (left) and F_{1b} (right), i. e. with identical and diametrical attitude of the mobile system.

However, the accuracies of the boresight angle β and the range offset d_0 vary for different configurations. Figure 4 shows the correlations of the calibration parameters for the configurations F_{1a} and F_{1b}, i. e. with identical and diametrical attitude of the mobile laser scanning system. It is evident that there are no parameter correlations in field F_1, except for β and d_0 when the reference planes are not scanned diametrically. This correlation has a magnitude of 31 %. This holds true for field F_2, where the correlation between β and d_0 reaches 23 %, when the scans are not performed diametrically (not shown in Figure 4). Hence, the diametrical scanning of the reference planes leads to a decorrelation of the parameters improving their accuracies. Table 2 also indicates that the accuracy of β is generally better in field F_1, whether or not the planes are scanned diametrically. This cannot be referred to correlations since in both fields there are no correlations left when the scans are executed diametrically. In this case, the reliability of the observations impacts on σ_β. Thus, the configurations were also analyzed with criteria for the internal and external reliability (Section 4.1.3).

4.1.3 Analysis with reliability criteria

The internal reliability of a network can be assessed with partial redundancies r_i describing the contribution of a single observation l_i to the total redundancy r, i. e. $\Sigma r_i = r$. The partial redundancies are calculated from Equation (7) where $\boldsymbol{\Sigma}_{vv}$ is the covariance matrix of the residuals $\boldsymbol{v}$. They indicate how well an observation is controlled within the network, i. e. to what extent deviations and gross errors impact on the own residual v_i rather than on other residuals or on the parameters (FÖRSTNER 1979, FÖRSTNER 1987). The partial redundancies are a measure for the controllability of a network within the observation domain.

$$r_i = tr\left(\boldsymbol{\Sigma}_{vv}\boldsymbol{\Sigma}_{ll}^{-1}\right) = tr\left(\boldsymbol{\Sigma}_{ll}\boldsymbol{B}^T\boldsymbol{\Sigma}_{\bar{l}\bar{l}}^{-1}\left(\boldsymbol{I} - \boldsymbol{A}\left(\boldsymbol{A}^T\boldsymbol{\Sigma}_{\bar{l}\bar{l}}^{-1}\boldsymbol{A}\right)^{-1}\boldsymbol{A}^T\boldsymbol{\Sigma}_{\bar{l}\bar{l}}^{-1}\right)\boldsymbol{B}\right) \qquad \in [0,1] \tag{7}$$

This is closely linked to the concept of the minimum detectable gross error ∇l_i of an observation and its impact $\nabla \boldsymbol{p}_i$ on the estimated parameters. This is generally known as external reliability, because the network controllability within the parameter domain is described (BAARDA 1967, BAARDA 1968). In Equation (8) the minimum detectable gross error ∇l_i of an observation that can be detected in an outlier test is calculated. The item δ_0 is called non-centrality parameter. It depends on the significance level α_T of the outlier test (probability of a type I error) and the power of the test β_T (probability of a type II error). For standardized values of $\alpha_T = 0.001$ and $\beta_T = 0.20$ one has $\delta_0 \approx 4.13$. From Equation (8) it can be seen that for a predefined non-centrality parameter δ_0 and a given accuracy σ_{li} of the observation the magnitude of ∇l_i depends on partial redundancy r_i of the observation. Therefore, higher partial redundancies increase the probability of detecting a gross error, which improves the reliability and controllability of the network configuration.

$$\nabla l_i = \delta_0(\alpha_T, \beta_T) \cdot \frac{\sigma_{l_i}}{\sqrt{r_i}} \tag{8}$$

By means of Equation (9) the impact $\nabla \boldsymbol{p}_i$ of an undetected gross error ∇l_i on the parameter estimation can be calculated. In this way, it can be analyzed how weakly controlled observations may corrupt the parameter estimation.

$$\nabla \boldsymbol{p}_i = \left(\boldsymbol{A}^T\boldsymbol{\Sigma}_{\bar{l}\bar{l}}^{-1}\boldsymbol{A}\right)^{-1}\boldsymbol{A}^T\boldsymbol{\Sigma}_{\bar{l}\bar{l}}^{-1}\left(\boldsymbol{B}\,[0,\cdots,\nabla l_i,\cdots,0]^T\right) \tag{9}$$

Table 3: Impact $\nabla \boldsymbol{p}_j$ of an undetected gross error $\nabla\theta_j$ on the estimation of the calibration parameters for the four network configurations (F_{1a}, F_{1b}, F_{2a} and F_{2b}).

Gross error	$\nabla_{\Delta x}$	$\nabla_{\Delta y}$	$\nabla_{\Delta z}$	∇_{α}	∇_{β}	∇_{γ}	∇_{d0}
F_{1a}: $\nabla\theta_j$ = **0.0464°**	0.02 mm	0.00 mm	0.11 mm	0.0000°	**-0.0077°**	0.0000°	0.00 mm
F_{2a}: $\nabla\theta_j$ = **0.0637°**	0.03 mm	0.00 mm	0.15 mm	0.0000°	**-0.0108°**	0.0000°	0.00 mm
F_{1b}: $\nabla\theta_j$ = **0.0471°**	0.02 mm	0.00 mm	0.10 mm	0.0000°	**-0.0078°**	0.0000°	-0.01 mm
F_{2b}: $\nabla\theta_j$ = **0.0658°**	0.03 mm	0.00 mm	0.15 mm	0.0000°	**-0.0111°**	0.0000°	0.00 mm

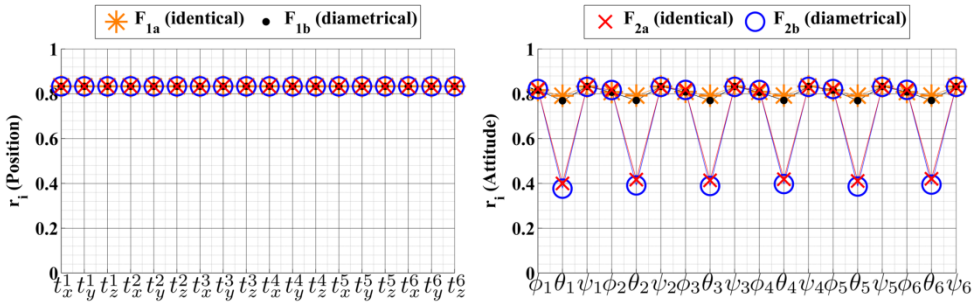

Fig. 5: Partial redundancies r_i of the position and attitude observations of the mobile laser scanning system for the four simulated configurations (F_{1a}, F_{1b}, F_{2a} and F_{2b}).

Figure 5 shows the partial redundancies r_i of the position and attitude observations of the mobile system for all six stations in each of the four configurations. In the left graph it can be seen that the partial redundancies of the positions uniformly reach values of about 0.83. This value is very high indicating a good controllability of the positions. Note that the value 0.83 depends on the number of stations S_j in the field, i. e. $r_i \approx 1 - (1 / \Sigma S_j)$ – quite similar to the accuracy of the calibration parameters in Equation (6).

However, the partial redundancies of the attitudes in the right graph show a totally different behavior. In the configurations F_{2a} and F_{2b} the partial redundancies of the pitch angles θ_j are clearly smaller than those of roll ϕ_j and yaw ψ_j, which again reach values of about 0.83. Accordingly, the pitch angles are weaker controlled by the configuration meaning that gross errors may not be detected and impact on the parameters. In this case the boresight angle β is worst affected, because β and θ_j rotate about similarly oriented axes (Figure 2). This is also evident from Table 3 where the minimum detectable gross error $\nabla\theta_i$ in one of the pitch angles and its impact $\nabla \boldsymbol{p}_i$ on the estimation of the calibration parameters is shown for all four configurations. It can be seen that the minimum detectable gross error is bigger for the configurations F_{2a} and F_{2b} due to the smaller partial redundancies. Moreover, it is evident that an undetected gross error $\nabla\theta_j$ in one of the pitch angles primarily impacts on the estimation of β – although there is a minor impact on Δz. In field F_2 the impact on β is even more critical. Coming back to the findings in Table 2 that the accuracy of the boresight angle β is generally better in field F_1 – the poorer controllability of the pitch angles θ_j in field F_2 is the reason why σ_β is worse in field F_2. On the basis of these simulations configuration F_{1b} was selected for the real system calibration (Section 4.2).

4.2 Calibration results on real data

Based on the simulations (Section 4.1) the configuration F_{1b} was realized to calibrate the mobile system (Section 2). Eight white reference planes (0.6 m × 0.9 m) were scanned with a high-end 3D laser scanner (Leica ScanStation P20) from the center of the field (Figure 6). This scan was georeferenced by using five GNSS control points, which had been measured statically for 2.5 hours. The GNSS conditions around the field were excellent, i. e. almost unobstructed horizon. Thus, the discrepancies at the control points after the georeferencing were ≤ 2 mm. The scanned points were transformed to a north-oriented l-frame located in the origin of the 3D laser scanner. Then, the reference planes were statically scanned with the mobile system from 30 diametrical stations from the center of the field (Figure 6).

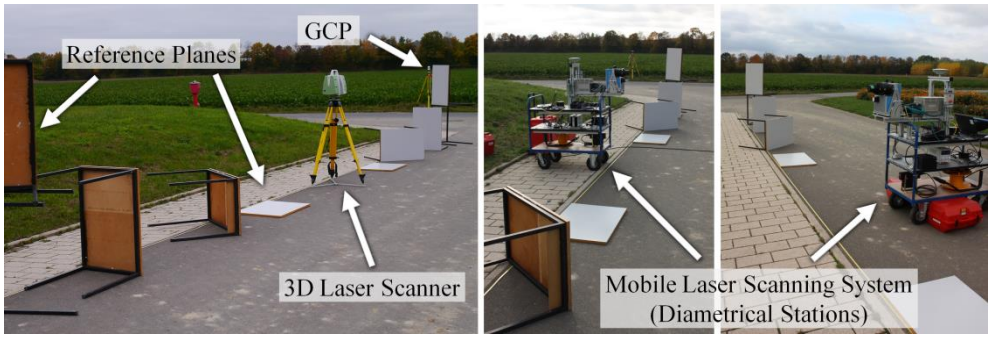

Fig. 6: Calibration field with eight reference planes. The field was georeferenced by using a 3D laser scanner Leica ScanStation P20 and GNSS control points (GCP). Then, the planes were scanned from several diametrical stations with the mobile system.

Due to an error in the data acquisition one scan was not usable. By means of the remaining 29 stations the estimation of the calibration parameters was carried out (Section 3). For the stochastic model $\boldsymbol{\Sigma}_{ll}$ manufacturer specifications were used (Table 1). This seems to be a reasonable assumption, because the global test of the adjustment displayed no model errors. The calibration results are summarized in Table 3. As can be seen, the boresight angles and the components of the lever arm each have the same accuracy, which is $\sqrt{29} \approx 5.4$ times better than the accuracy of the position and attitude observations of the INS. Each static scan with the mobile system took about 60 seconds. In the adjustment the observed position and attitude of the INS were averaged for this time interval, which reduces the noise. Thus, the accuracy of the calibration can be assumed to be more than five times better than the accuracy of the mobile system. The range offset d_0 of the 2D laser scanner was significantly estimated with 0.7 mm. Yet, due to neglected correlations the parameter accuracies might be too optimistic, this specifically applies to σ_{d0} due to the high redundancy.

Tab. 3: Calibration results for the real mobile system (STD: standard deviation).

Parameter	α	β	γ	Δx	Δy	Δz	d_0
Value	0.2170°	0.1799°	-0.1817°	-0.7957 m	0.0448 m	0.1731 m	0.70 mm
STD (1σ)	0.0019°	0.0019°	0.0019°	0.0019 m	0.0019 m	0.0019 m	0.01 mm

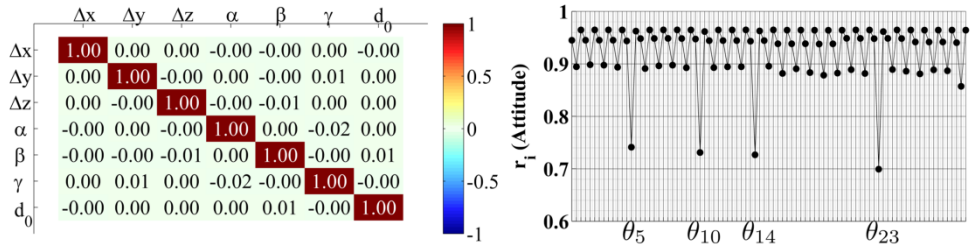

Fig. 7: Correlations of the calibration parameters in the calibration field (left) and partial redundancies of the attitude observations of the INS (right).

Figure 7 indicates that there are no parameter correlations and that the partial redundancies reach high values as was expected from the simulations. The observed positions, which are not depicted in Figure 7, uniformly reached a value of about 0.97, i. e. $r_i \approx 1 - (1/29)$. The variation of the partial redundancies of the observed attitudes in Figure 7 is most probably caused by the fact that the network configuration was not exactly realized as simulated. However, the values of four pitch angles $\theta_{5,\,10,\,14,\,23}$ are considerably smaller than the others. Regarding the stations $S_{5,\,10,\,14,\,23}$ either plane P_1 or plane P_8 was not hit by the laser beam, which worsens the network configuration. In summary, it can be stated that the calibration results are consistent with the simulations in Section 4.1.

5 Evaluation of the System

To evaluate the mobile system two kinematic scans of the Poppelsdorfer Schloss in Bonn were conducted. The southern façade of the building was first scanned from left to right and then once again in opposite direction from right to left with the system having been turn by 180° with respect to its vertical axis. By using Cloud Compare (CLOUD COMPARE 2016) a comparison of the two point clouds was made based on an M3C2 point cloud distance. According to LAGUE et al. (2013), who developed this special distance measure for point clouds, the M3C2 distance is based on the estimation and orientation of surface normals at a scale consistent with the local surface roughness. The distance is then calculated along the directions of these normals. More details about this can be found in LAGUE et al. (2013).

The results of the comparison are shown in Figure 8. From the histogram it can be seen that the deviations δ between the two point clouds are mainly in the range between ± 3 cm. The RMS (route-mean-square error) of the deviations is 2.75 cm. In the histogram no systematic effects are apparent since the deviations evenly spread around zero. However, when having a look at the scattered deviations δ of the point clouds below, remaining systematic effects are visible, e. g. at the right side of the outside staircase. We suggest that an inadequately estimated trajectory of the system in this area is the reason for this. Currently, the trajectory is estimated by utilizing a basic algorithm without a sophisticated modeling of the platform motion. In the future the trajectory estimation algorithm will be optimized and the remaining systematic deviations in the 3D point clouds will be further investigated. Next to the histogram, a top view of the left pillars of the façade is shown. The two point clouds show a good overlapping. Thus, despite the local systematic deviations, the quality of the captured 3D point clouds of the mobile laser scanning system is satisfactory.

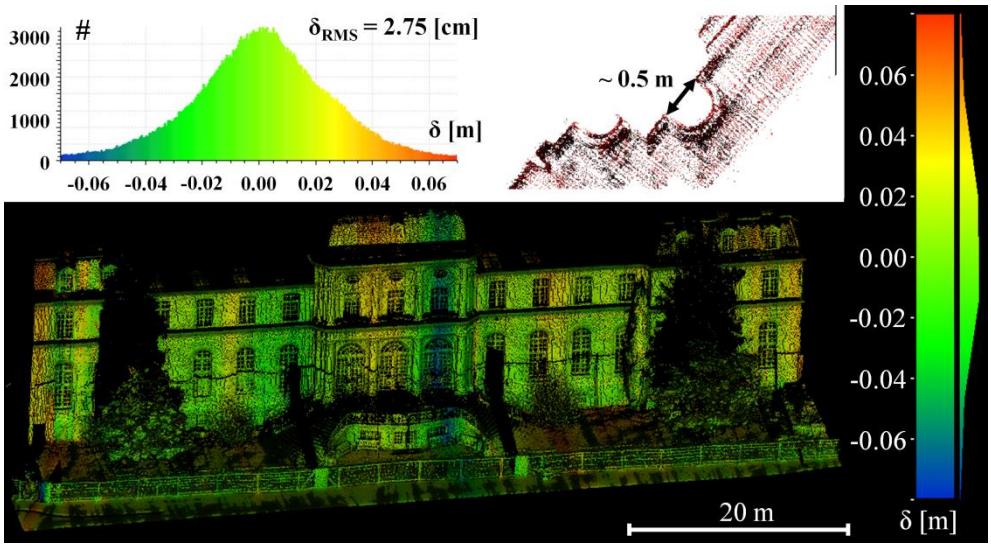

Fig. 8: Comparison of two kinematic scans of the Poppelsdorfer Schloss in Bonn. The top view of the pillars at the façade indicates a good overlapping of the point clouds.

6 Conclusions

In this work, a plane-based approach for the calibration of a mobile laser scanning system was addressed. The configuration of the calibration field was determined on the basis of an in-house developed simulation tool (i. e. the setup of the reference planes and how they are scanned with the mobile system). The simulation showed that parameter correlations and weakly controlled observations can corrupt the quality of the calibration results in the case of a poor configuration. If the configuration is good, both the range offset and the extrinsic calibration parameters of the 2D laser scanner can be reliably determined. The accuracy of the calibration depends on the accuracy of the position and attitude observations of the system and the number of stations of the system in the calibration field. The application to a real mobile laser scanning system confirmed the simulated results. This led to a successful calibration of all calibration parameters with an accuracy that was about five times better than the measuring accuracy of the system. The system evaluation showed that the accuracy of a 3D point cloud captured with the system is in the order of a few cm.

However, systematic deviations are left in the 3D point clouds, which can most probably be traced back to the trajectory estimation algorithm. In the future, this will be further investigated. Regarding the calibration, it will be analyzed if other intrinsic calibration parameters of the 2D laser scanner can be included. Moreover, it will be examined how the network has to be designed if the architecture of the mobile system changes, e. g. a tilt of 45° of the 2D laser scanner as common in many systems. Beyond that, the refinement of the stochastic model of the observations could lead to a more realistic estimation for the parameters and the parameter accuracies. The authors are currently working on the realization of a test field for the calibration and evaluation of kinematic multi sensor systems.

References

BAARDA, W. (1967): Statistical Concepts in Geodesy. In: Netherlands Geodetic Commission, Publications on Geodesy, New Series, Volume 2, Number 4.

BAARDA, W. (1968): A Testing Procedure for Use in Geodetic Networks. In: Netherlands Geodetic Commission, Publications on Geodesy, New Series, Volume 2, Number 5.

CHAN, T. O., LICHTI, D. D., GLENNIE, C. L. (2013): Multi-feature based boresight self-calibration of a terrestrial mobile mapping system. In: ISPRS Journal of Photogrammetry and Remote Sensing 82, pp. 112-124.

CLOUD COMPARE (2016): CloudCompare - 3D Point Cloud and Mesh Processing Software, Open Source Project. http://www.cloudcompare.org (23.12.2016).

COPPELIA ROBOTICS (2016): Virtual Robot Experimentation Platform (v-rep). http://www.coppeliarobotics.com (23.12.2016).

ELING, C., KLINGBEIL, L. & KUHLMANN, H. (2015): Real-time single-frequency GPS/MEMS-IMU attitude determination of lightweight UAVs. In: Sensors 15, pp. 26212-26235.

FILIN, S. (2003): Recovery of Systematic Biases in Laser Altimetry Data Using Natural Surfaces. In: Photogrammetric Engineering & Remote Sensing 69 (11), pp. 1235-1242.

FÖRSTNER, W. (1979): Das Programm TRINA zur Ausgleichung und Gütebeurteilung geodätischer Lagenetze. In: Zeitschrift für Vermessungswesen (ZfV) 104 (2), pp. 61-72.

FÖRSTNER, W. (1987): Reliability Analysis of Parameter Estimation in Linear Models with Applications to Mensuration Problems in Computer Vision. In: Computer Vision, Graphics and Image Processing 40, pp. 273-310.

GLENNIE, C. (2012): Calibration and Kinematic Analysis of the Velodyne HDL-64E S2 Lidar Sensor. In: Photogrammetric Engineering & Remote Sensing 78 (4), pp. 339-347.

GRAFAREND, E. W. & SANSÒ, F., eds. (1985): Optimization and Design of Geodetic Networks. Springer Verlag. Berlin, Heidelberg, New York, Tokyo.

GRÄFE, G. (2007): High precision kinematic surveying with laser scanners. In: J. Appl. Geodesy 1 (4), pp. 185-199.

GROVES, P. D. (2013): Principles of GNSS, Inertial, and Multisensor Integrated Navigation Systems (2nd Edition). Artech House. Boston, London.

HARTMANN, J., PAFFENHOLZ, J.-A., STRÜBING, T. & NEUMANN, I. (2015): Determination of Position and Orientation of LIDAR-Sensors on Multi-Sensor Platforms. In: Proceedings of the 9th International Symposium on Mobile Mapping Technology (MMT), Sydney, Australia, December 9-11, 2015.

HAUSER, D., GLENNIE, C. & BROOKS, B. (2016). Calibration and Accuracy Analysis of a Low-Cost Mapping-Grade Mobile Laser Scanning System. In: Journal of Surveying Engineering 142 (4) (04016011-1 – 04016011-9).

HEINZ, E., ELING, C., WIELAND, M., KLINGBEIL, L. & KUHLMANN, H. (2015): Development, Calibration and Evaluation of a Portable and Direct Georeferenced Laser Scanning System for Kinematic 3D Mapping. In: J. Appl. Geodesy 9 (4), pp. 227-243.

HEINZ, E., ELING, C., WIELAND, M., KLINGBEIL, L. & KUHLMANN, H. (2016): Development, of a Portable Mobile Laser Scanning System with Special Focus on the System Calibration and Evaluation. In: Proceedings of the 5th International Conference on Machine Control and Guidance (MCG), Vichy, France, October 5-6, 2016.

HOLST, C., ELING, C. & KUHLMANN, H. (2013): Automatic optimization of height network configurations for detection of surface deformations. In: J. Appl. Geodesy 7 (2), pp. 103-113.

HOLST, C. & KUHLMANN, H. (2014): Aiming at self-calibration of terrestrial laser scanners using only one single object and one single scan. In: J. Appl. Geodesy 8 (4), pp. 295-310.

HOLST, C., NEUNER, H., WIESER, A., WUNDERLICH, T. & KUHLMANN, H. (2016): Calibration of Terrestrial Laser Scanners. In: Allgemeine Vermessungs-Nachrichten (AVN) 6/2016, pp. 147-157, Wichmann Verlag, Berlin.

IMAR (2016): Inertial Navigation System iNAV-FJI-LSURV. http://www.imar.de/index.php/en/products/by-product-names (23.12.2016).

JIAN, Z. & RAVANI, B. (2016): Boresight Calibration of Mobile Laser Scanner Using an External Fixture. In: J. Appl. Geodesy 10 (3), pp. 175-183.

KELLER, F. & STERNBERG, H. (2013): Multi-Sensor Platform for Indoor Mobile Mapping: System Calibration and Using a Total Station for Indoor Applications, In: Remote Sensing 5, pp. 5805-5824.

KLINGBEIL, L., ELING, C., ZIMMERMANN, F. & KUHLMANN, H. (2014): Magnetic Field Sensor Calibration for Attitude Determination. In: J. Appl. Geodesy 8 (2), pp. 97-108.

KUHLMANN, H., SCHWIEGER, V., WIESER, A. & NIEMEIER, W. (2014): Engineering Geodesy - Definition and Core Competencies. In: J. Appl. Geodesy 8 (4), pp. 327-333.

LAGUE, D., BRODU, N. & LEROUX, J. (2013): Accurate 3D comparison of complex topography with terrestrial laser scanner: Application to the Rangitikei canyon (N-Z). In: ISPRS Journal of Photogrammetry and Remote Sensing 82 (2013), pp. 10-26.

MARTIN, H., GROVES, P. & NEWMAN, M. (2016): The Limits of In-Run Calibration of MEMS Inertial Sensors and Sensor Arrays. In: Navigation 63 (2), pp. 127-143.

MIKHAIL, E. M. & ACKERMANN, F. E. (1976): Observations and Least Squares. Dun-Donnelley Publisher, New York.

OLSEN, M. J., ROE, G. V., GLENNIE, C., PERSI, F., REEDY, M., HURWITZ, D., WILLIAMS, K., TUSS, H., SQUELLATI, A. & KNODLER, M. (2013): Guidelines for the Use of Mobile LIDAR in Transportation Applications. In: National Cooperative Highway Research Program (NCHRP) Report 748, National Academy of Sciences, Washington, D. C.

PUENTE, I., GONZÁLEZ-JORGE, H., MARTÍNEZ-SÁNCHEZ, J. & ARIAS, P. (2013): Review of mobile mapping and surveying technologies. In: Measurement 46, pp. 2127-2145.

RIEGER, P., STUDNICKA, N., PFENNIGBAUER, M. & ZACH, G. (2010): Boresight alignment method for mobile laser scanning systems. In: J. Appl. Geodesy 4 (1), pp. 13-21.

SKALOUD, J. & LICHTI, D. (2006): Rigorous approach to bore-sight self-calibration in airborne laser scanning, In: ISPRS Journal of Photogrammetry and Remote Sensing 61 (2006), pp. 47-59.

TALAYA, J., ALAMUS, R., BOSCH, E., SERRA, A., KORNUS, W. & BARON, A. (2004): Integration of a terrestrial laser scanner with GPS/IMU orientation sensors. In: Proceedings of the 20th ISPRS Congress (2004).

TITTERTON, D. H., WESTON, J. L. (2004): Strapdown Inertial Navigation Technology (2nd Edition). The Institute of Electrical Engineers.

WÜBBENA, G., SCHMITZ, M., MENGE, F., BÖDER, V. & SEEBER, G. (2000): Automated absolute field calibration of GPS antennas in real-time. In: Proceedings of the International Technical Meeting, ION GPS-00, Salt Lake City, USA, September 19-22, 2000.

ZEIMETZ, P. & KUHLMANN, H. (2008): On the Accuracy of Absolute GNSS Antenna Calibration and the Conception of a New Anechoic Chamber. In: Proceedings of the FIG Working Week 2008, June 14-19, Stockholm, Sweden.

ZOLLER + FRÖHLICH (2016): Z+F Profiler® 9012, 2D Laser scanner. http://www.zf-laser.com/Z-F-PROFILER-R-9012.2d_laserscanner.0.html?&L=1 (23.12.2016).